Application of reconstructed phase-space techniques for correlation-dimension calculations in a spatially extended dynamical system

J. J. Żebrowski

Institute of Physics, Warsaw University of Technology, ul.Koszykowa 75, PL00-662 Warszawa, Poland

(Received 28 July 1992)

The correlation dimension is calculated for data from a partial-differential-equation model of a magnetic-domain wall—the Bloch wall in a magnetic thin film. The data were extracted from different locations along the height of the wall and two types of embedding were used: a time-delay method from data taken at a single location in the wall (reconstructed phase space) and data taken from ten locations in the wall simultaneously (physical phase space). Three chaotic attractors of the Bloch wall were studied. The time-delay method for some attractors gives a dependence of the correlation dimension on the location at which the data were extracted. This dependence has a specific symmetry with respect to the film in which the Bloch wall resides and a surface (or boundary) effect is seen—the correlation dimension is different at the surfaces of the film. Several scaling regions are found in some cases. The physical phase-space embedding yields a correlation dimension which is an average of the spatial dependence obtained in the time-delay method, but usually this embedding gives a somewhat lower value of the correlation dimension.

I. INTRODUCTION

Many deterministic physical systems exhibit chaotic dynamics. Of these some are described by ordinary differential equations of motion (e.g., the nonlinear oscillator, the Lorenz systems, and the Bielousov-Zhabotinski chemical reaction [1]) and much fewer systems are described by partial differential equations of motion (e.g., the Navier-Stokes hydrodynamic equation [1], the sine-Gordon-equation soliton system [2], and the Bloch magnetic-domain wall [3,4]). In the latter type of systems, not only temporal deterministic chaos but also spatiotemporal chaos is possible.

For the ordinary-differential-equation systems a number of well-tested tools for nonlinear dynamics analysis of their behavior exist. Among others, algorithms for the calculation of Liapunov exponents [5], $f(\alpha)$ curves [6], and correlation dimensions [7] are readily available. In most cases, however, all calculations are done not in the original phase space of the system but in a synthetic phase space reconstructed from a single, arbitrarily chosen variable of the system by a time-delay technique based on an embedding theorem by Takens [8,9]. There is, of course, an excellent reason for such an approach as, especially in dealing with experimental data, usually not all variables are available.

The effect of information flow in spatially extended systems (described by coupled maps) has been studied [10,11] and it was demonstrated that local dynamics creates a perturbation the effect of which may diffuse along the spatial directions of the system. The question then arises as to how fast the amplitude of the information decays with distance. Moreover, given a finite resolution due to the finite length of the time series, how strongly will a remote dynamical event be felt in other parts of the system by the analysis technique of choice?

Following an idea by Pomeau [12], Kurtz and Mayer-Kress [13,14] have measured a two-point dimension density calculated from a combined signal taken from two points in the system some distance apart. Both in [12] and in [13,14] the reader is cautioned that the method may be applied only to systems in which the dynamics is sufficiently independent of position (homogeneous dynamics). In spite of this rather strong assumption, the results show clearly that, for a given coupling strength between the lattices of the system, the local dynamics at one point are felt at other points in the system only within a finite distance.

The magnetic-domain wall of the Bloch type [3,4], which was the spatially extended system studied here, is not homogeneous in the sense that it not only has boundaries (the surfaces of the thin film of a uniaxial magnetic material in which it resides [3]), but also the distance between these boundaries is such that the dynamics between them is strongly influenced by them. A surface effect may be obtained for some areas of parameter space and the phase portraits calculated from a point in the wall located at the surface of the film are different from those deeper inside the material [15]. For such a system the time-delay reconstruction technique is not obviously an adequate tool to find a global measure of the dynamics in the system (e.g., a single correlation-dimension value).

In this paper a comparison is made between the correlation dimension calculated in phase spaces reconstructed by means of data taken from several locations along the magnetic-domain wall with the correlation dimension calculated for the trajectory of the wall in physical phase space. It is shown that in a spatially extended system with inhomogeneous dynamics like the Bloch wall studied here, the use of the single-point time-delay reconstruction technique may be a probe of the number of degrees of freedom active at a given location in the system.

Single-point correlation dimension is treated as a measure of the local dynamics of the system. The results indicate that the spatial distribution of the correlation dimension is related to the symmetry of the system: the number of degrees of freedom is, in general, decreased at the boundaries of the system and at the midplane of the system. The multiscale character of the chaotic attractors studied is discussed. The correlation dimension calculated from single-point time-delay reconstruction of the attractors is compared with the same quantity calculated from a physical phase space (for definition, see below) and it is shown that, in general, the results are not the same.

II. THE PHYSICAL SYSTEM

The calculations were carried out for a spatially extended dynamical system: a magnetic-domain wall of the Bloch type (Fig. 1). This is the simplest of all possible 180° magnetic-domain walls [16]. For magnetic materials with a uniaxial anisotropy energy density which is larger than the demagnetization energy density, the wall may be treated as a membrane of magnetic moments (the Bloch surface) with an additional degree of freedom—the azimuthal angle of the magnetic moment with respect to this membrane [3,16]. Then the equations of motion are

$$\dot{q} = \gamma \Delta \left[2\pi M \sin(2\varphi) - \frac{2A}{M} \frac{\partial^2 \varphi}{\partial z^2} \right] + \alpha \Delta \dot{\varphi} \ ,$$

$$\dot{\varphi} = \gamma \left[H_z + \frac{2A}{\Delta M} \frac{\partial^2 q}{\partial z^2} \right] - \alpha \frac{\dot{q}}{\Delta} \ ,$$

where A is the exchange constant, γ is the gyromagnetic ratio, $4\pi M$ is the saturation magnetization, Δ is the Bloch wall width, α is the Gilbert damping constant, and H_z is the constant drive field. $q(z,t)$ is the local position of the wall, the azimuthal angle $\varphi(z,t)$ describes the position of the magnetic moment with respect to the plane of the wall, and the axis of the coordinate z lies in the plane of the wall and is parallel to the easy axis of the anisotropy. For all cases studied in this paper, the easy axis of the anisotropy was assumed to be perpendicular to the surface of the magnetic material in which the domains reside and the surface stray fields were ignored (see discussion in Ref. [3]). The equations of motion of the wall were solved by means of a numerical scheme which is a version of the well-known DuFort-Frankel method rewritten in
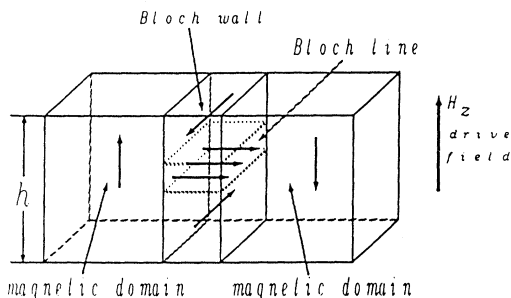
vector form [3]. In the calculations discussed below, depending on the height of the wall, from 52 to 88 evenly spaced numerical grid points were used with a 0.05-ns time step.

Force-free boundary conditions [3] $\partial q / \partial z = 0$ and $\partial \varphi / \partial z = 0$ were applied. The initial conditions were $q(z,0) = 0.0$ and $\varphi(z,t) = 0.0$.

The material parameters were the following: exchange constant $A = 0.81 \times 10^{-7}$ erg/cm, saturation magnetization $4\pi M = 140G$, gyromagnetic ratio $\gamma = 1.73 \times 10^7$ 1/s Oe, Bloch wall width $\Delta = 0.029 \times 10^{-4}$ cm, Gilbert damping constant $\alpha = 0.156$. For these material parameters the Walker critical field, which separates two distinct regimes of the motion of the Bloch wall, is $H_w = \alpha 2\pi M = 10.92$ Oe; below H_w a stationary motion is obtained while for drive field magnitudes larger than the critical value periodic or chaotic states are possible [3].

It has been known for some time—from experiments on domain wall dynamics [16] and from different theoretical discussion (cf. [13])—that the Bloch wall moving in a spatially uniform drive field of a larger value than the threshold of the Walker field will divide itself into parts separated by solitary-wave-like kinks [19] which propagate along the wall surface. If the height of the wall is not too large, the resulting dynamic state may be periodic [3]. An example of such a case for wall height $h = 3$ μm is shown in Fig. 2 and the corresponding phase portrait
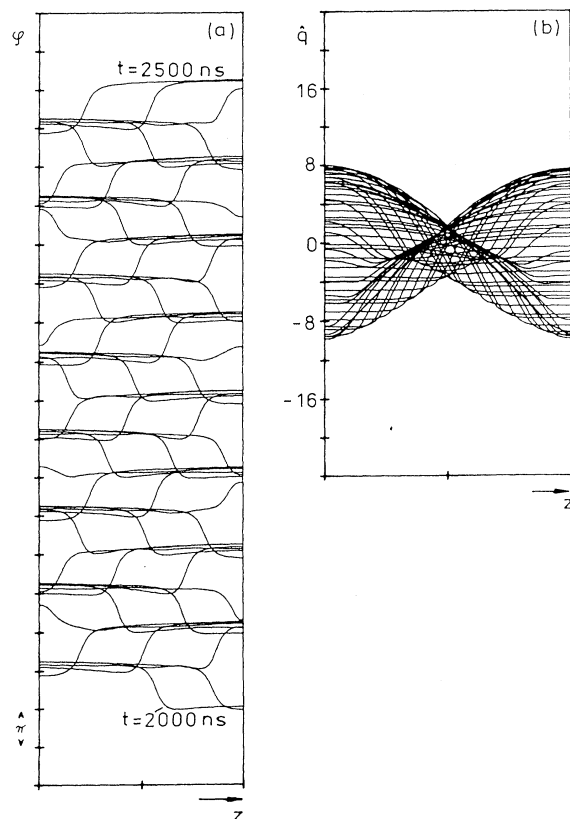

FIG. 2. (a) Stationary-state time evolution of the wall structure $\varphi(z,t)$ and (b) wall surface shape $\hat{q}(z,t) = q(z,t) - q(t)$ for $h = 3.0$ μm; $q(t)$ is the spatial average of $q(z,t)$. All curves shown every 10 ns.

FIG. 1. 180° Bloch wall between two domains in a thin magnetic film with uniaxial perpendicular anisotropy.
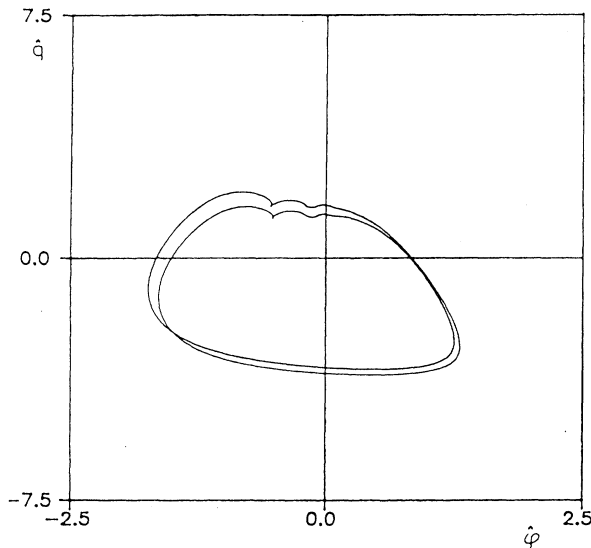
FIG. 3. Phase portrait of the midplane point in the wall in a frame moving with the spatial averages $q(t)$ and $\varphi(t)$ for the periodic attractor at $h = 3.0\,\mu$m.

(in a moving frame [3]) is shown in Fig. 3. However, once the height of the wall increases above a certain threshold (3.0 μm for the material parameters used here), the prevailing dynamic states of the wall will be chaotic [3] with only narrow periodic windows [19]. The strange attractors found above this threshold are the subject of this study.

III. PHASE SPACE

The phase space of a system described by a partial differential equation of motion is infinite dimensional. Since the spatial grid used for the calculations here contained from 52 to 88 grid points, the effective phase space for the pair of equations of motion of the Bloch wall was 104 to 176 dimensional. For every attractor studied, a subspace of the full phase space was saved for correlation-dimension calculations: the two variables $q(z,t)$ and $\varphi(z,t)$ from every fourth spatial grid point were stored.

The calculations were then carried out for the trajectory of the system embedded in two different kinds of space.

In the *physical space* the data for $q(z,t)$ was taken at ten evenly spaced locations from within the wall height. Because there are two variables this gave two ten-dimensional embedding spaces: a q space and a φ space; however, only results concerning the former will be presented here as the other embedding does not give qualitatively new results.

In the *reconstructed space* the data for the variable chosen [$q(z,t)$] was stored for chosen locations defined by the spatial grid point number. The data vector was then embedded in a ten-dimensional space constructed with a suitable time delay according to the theorem by Takens [8,9].

IV. CORRELATION DIMENSION

A slightly modified Grassberger-Procaccia algorithm was used to calculate the correlation dimension [7]. This algorithm requires that, given the matrix dimension, i.e., the dimension of the phase space used, the sum of the number of points belonging to the trajectory of the system and lying within a hypersphere of the radius ϵ surrounding each point of the trajectory [i.e., the correlation function $C(\epsilon)$] can be found:

$$C(\epsilon) = [1/(NP)] \sum_{i=1}^{N} \sum_{j>i+K}^{N} \Theta(\epsilon - |y(i) - y(j)|) \,,$$

with Θ the Heaviside function. The number K ensures that the vectors used in the calculations will be sufficiently independent [17]. In the present case it was found that if $K \geq 4$ no enhancement of the scaling region results. Also, to shorten the computer time, for summation over j a random representation of $P = 10\%$ of the total number of points N was chosen (cf. [18]). The correlation dimension is then just the slope—within a certain scaling region—of the logarithm of this number as the function of the logarithm of the radius ϵ of the hypersphere. The hypersphere radius ϵ was changed by factors of 2 so that the exponent of 2 could be extracted from the computer real number representation without resorting to calculations of logarithms. Euclidean norm was used (cf. [17]).

A large number of tests were carried out to find the proper sampling time which allows us to obtain a good scaling region, i.e., the range of ϵ for which the number of points scales exponentially with sphere size. The best sampling time for the states discussed here was found to be 2 ns (values ranging from 0.5 to 6 ns were used). Simultaneously it was found that, for two of the chaotic attractors studied, it is sufficient to use trajectories 10 000 ns long (5000 data points) to obtain a good estimate of the correlation dimension. 20 000-ns-long trajectories (10 000 data points) were also used with equally good re-
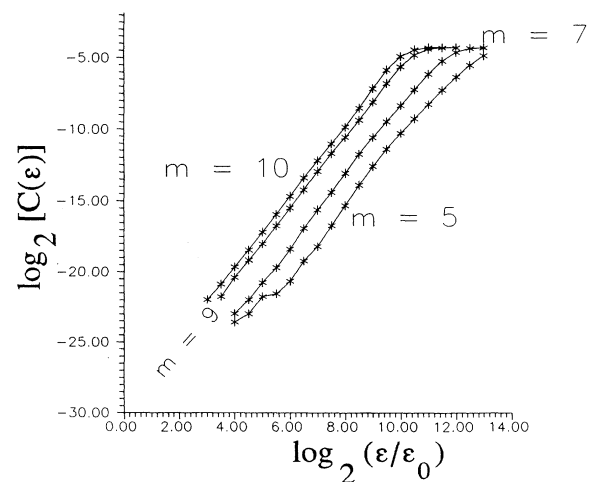

FIG. 4. Example of correlation function C vs hypersphere radius ϵ for several values of the matrix dimension m.

sults, but it was found that such a number of points yields results which are much clearer physically for the third attractor studied ($h = 5$ μm—see below).

The optimum matrix dimension was found to be 10 for both the physical phase space and the reconstructed phase space. As an example, the correlation function versus the radius ϵ in log-log scale is shown in Fig. 4 for matrix dimension $m = 5$, 7, 9, and 10 for physical phase-space calculation for one of the attractors studied here ($h = 4.5$ μm and data taken from grid point number 48). It can be seen that the slope of the curves saturates very well with the value of m so that $m = 10$ may be considered a sufficiently large embedding dimension.

For the case of the reconstructed phase space, an additional degree of freedom remains in the choice of the time delay τ. Using as basic criterion the linearity of the correlation function, it was found that the best results were obtained for delay time $\tau = 3$ ns [although values of τ ranging from 1 to 7 ns were tried with the shape of the $C(\epsilon)$ curve changing from concave to convex with τ; at the extreme values of this parameter no scaling regions could be defined].

V. RESULTS AND DISCUSSION

Three different chaotic attractors of the Bloch domain wall [3,15] were chosen as case studies. All are obtained for different wall height h, but the same value of the drive field $H_z = 12$ Oe, i.e., 1.08 Oe above the Walker critical field. For all attractors studied, the data were stored for the variable $q(z,t)$ and always with a time step of 1 ns for up to 20 000 ns after the transients had died out (at $t \leq 2000$ ns).

A. Reconstructed phase space

The chaotic attractor for wall height $h = 3.5$ Oe was found elsewhere [15] to be spatially uniform: the phase portraits of the time evolution of $q(z,t)$ versus $\varphi(z,t)$ for different spatial locations were very similar to each other as were the power spectra in the time domain at these points. The steady-state phase portrait for the midplane point of the wall for this case is seen in Fig. 5 while the
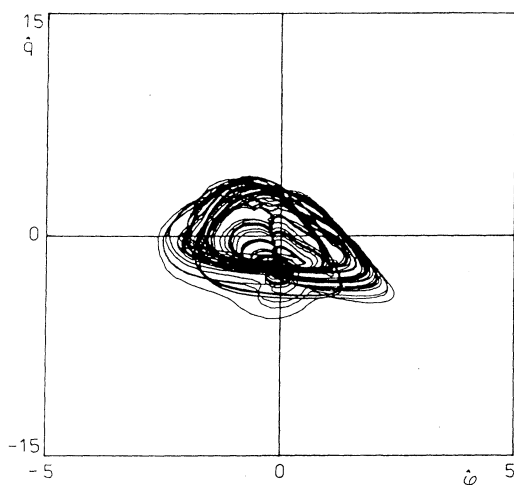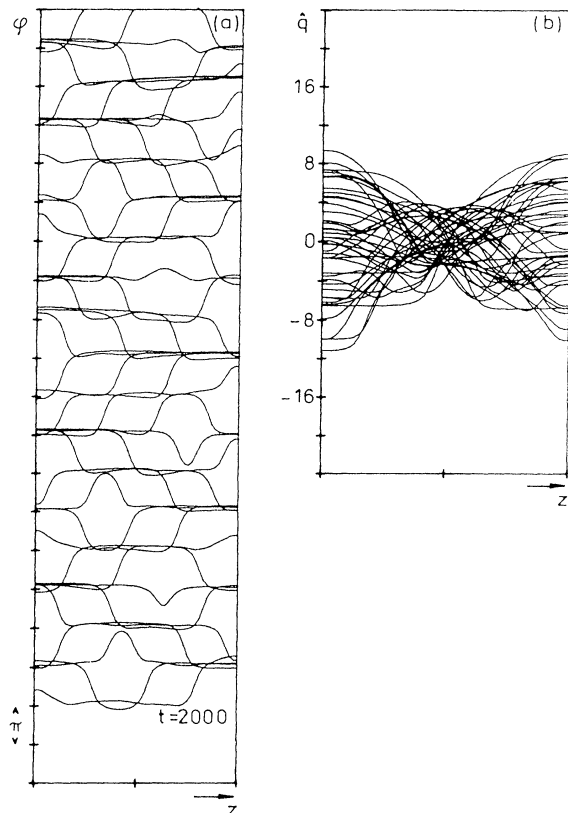
FIG. 6. (a) Stationary-state time evolution of the wall structure $\varphi(z,t)$ and (b) wall surface shape $\hat{q}(z,t) = q(z,t) - q(t)$ for $h = 3.5$ μm; $q(t)$ is the spatial average of $q(z,t)$. All curves shown every 10 ns.

wall structure $\varphi(z,t)$ and the wall surface shape $q(z,t)$ in a frame moving with the average position of the wall is seen in Figs. 6(a) and 6(b), respectively [15]. This is then a state in which two π-kink solitary-wave excitations (Bloch lines) [3,19] are present in the wall; the wall surface vibrates in an irregular way.
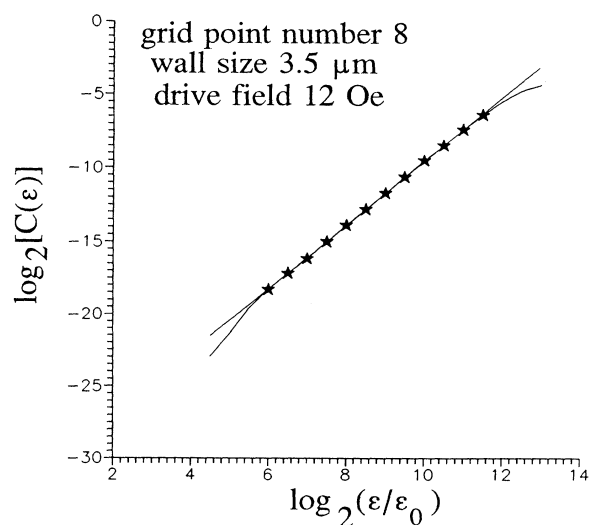
FIG. 5. Phase portrait of the midplane point in the wall for the chaotic attractor at $h = 3.5$ μm.

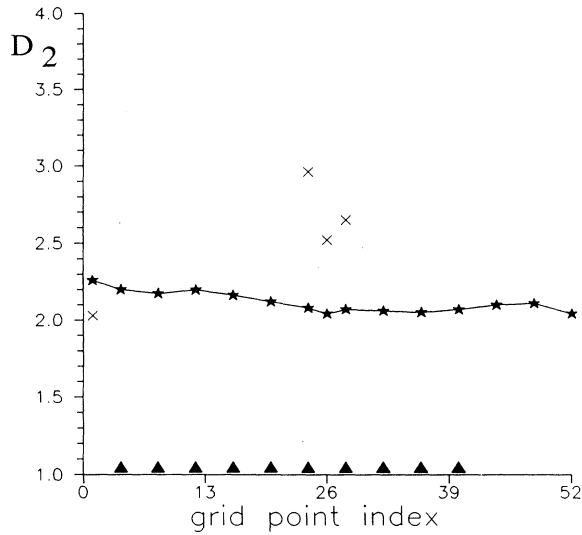FIG. 7. Correlation function $C(\epsilon)$ for $h = 3.5$ μm calculated at grid point number 8.

FIG. 8. Correlation dimension D_2 for $h = 3.5$ μm as function of position along the height of the wall. Symbols: $\times$, values obtained from the secondary scaling region at lower lengths scales; $\blacktriangle$, locations from which the physical space was constructed.

The correlation dimension calculated for the attractor of Figs. 5 and 6 in the phase space reconstructed at different spatial locations in the wall reflects the spatially uniform character of this state. Figure 7 depicts an example of the correlation function versus hypersphere radius obtained for this case. Figure 8 depicts the distribution of the correlation dimension along the wall height obtained for the phase space reconstructed from data taken at the grid points chosen. Although the value of the correlation dimension changes slightly from location to location, the differences are rather small and not much larger than the error, which is estimated to be about 0.1. Two interesting features are visible in Fig. 8. First, the value of the dimension at the surfaces is somewhat
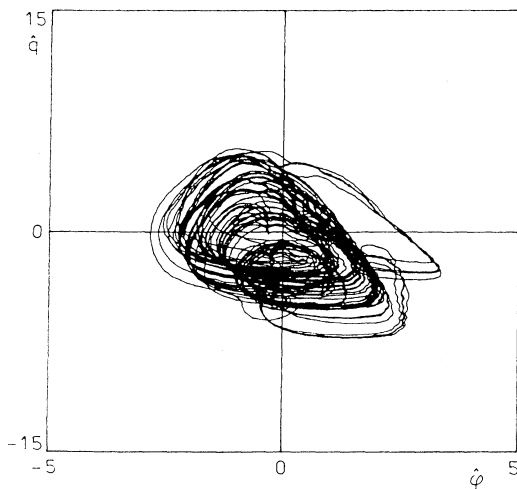

FIG. 9. Phase portrait of the midplane point in the wall for the chaotic attractor at $h = 4.5$ μm.
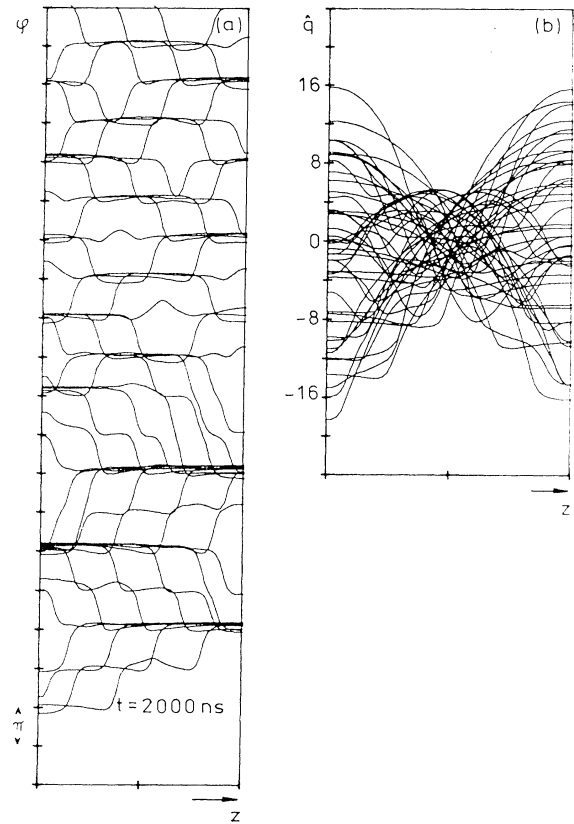

FIG. 10. (a) Stationary-state time evolution of the wall structure $\varphi(z,t)$ and (b) wall surface shape $\hat{q}(z,t) = q(z,t) - q(t)$ for $h = 4.5$ μm; $q(t)$ is the spatial average of $q(z,t)$. All curves shown every 10 ns.
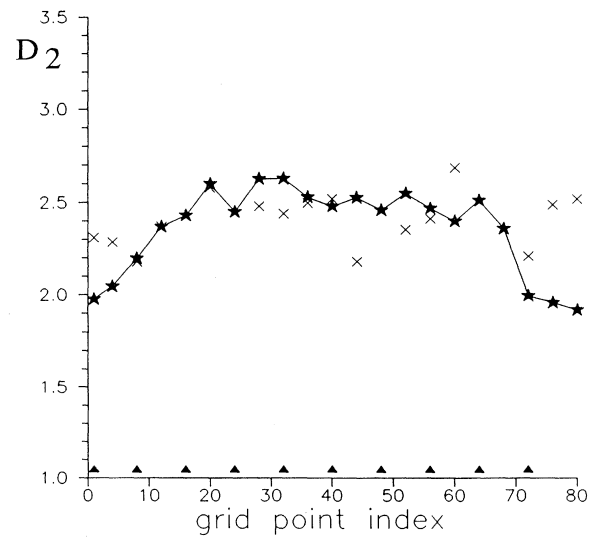

FIG. 11. Correlation dimension D_2 for $h = 4.5$ μm as function of position along the height of the wall. Symbols: $\times$, values obtained from the secondary scaling region at lower lengths scales: $\blacktriangle$, locations from which the physical space was constructed.
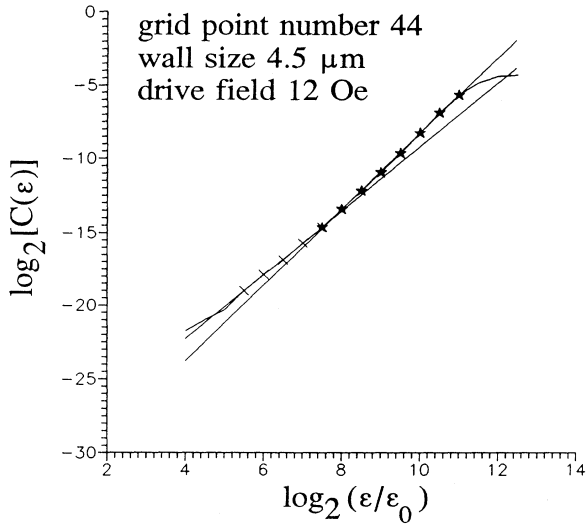
FIG. 12. Correlation function $C(\epsilon)$ for $h = 4.5\ \mu$m calculated at grid point number 44.

different from that obtained from phase-space reconstruction performed on data farther from the surface of the film and also these values are different at the two surfaces of the film. Second, an additional scaling region is found for data taken for several grids points (x in Fig. 8).

Considerable effort went into attempts at getting rid of this secondary scaling region by adjusting the parameters of the calculation: the sampling time and the time delay. It was found that the secondary scaling region is a persistent feature for the specific grid points where it is visible. At most what could be achieved in this way was that the additional scaling region was shorter and less well defined (less than three points), but it did not disappear. Usually, the only result of such a manipulation of the parameters of the computation was that the linearity of the function $C(\epsilon)$ was completely lost. Because of this behavior the second scaling region is considered to be a
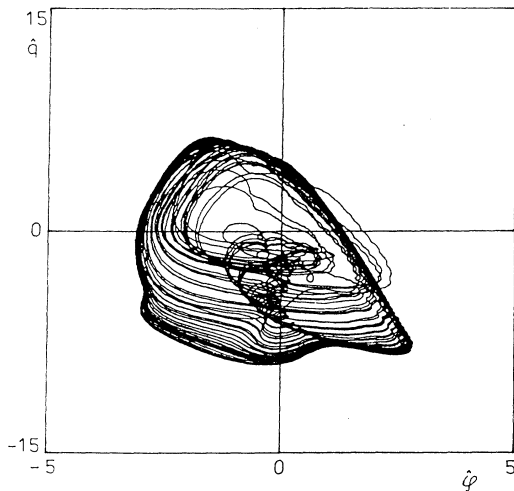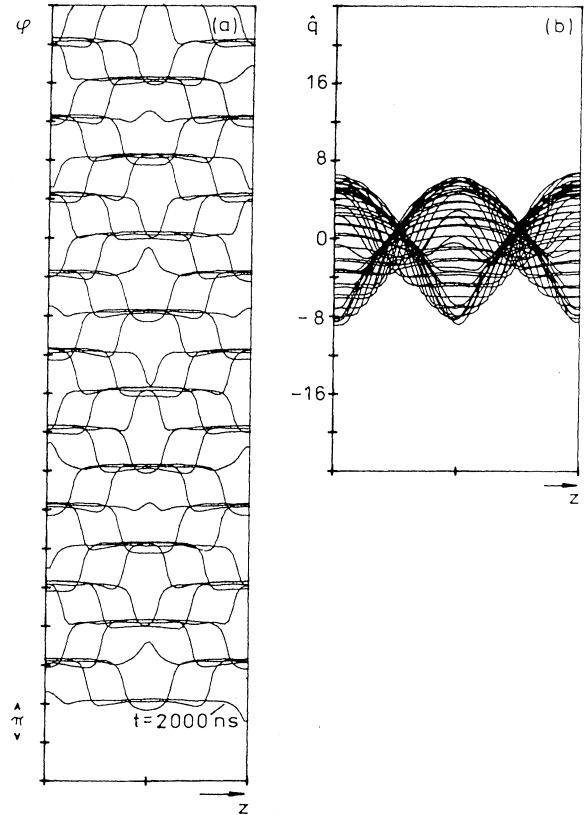

FIG. 14. (a) Stationary-state time evolution of the wall structure $\varphi(z,t)$ and (b) wall surface shape $\hat{q}(z,t) = q(z,t) - \overline{q}(t)$ for $h = 5.0\ \mu$m; $\overline{q}(t)$ is the spatial average of $q(z,t)$. All curves shown every 10 ns.

feature of the attractors studied and not an artifact.

The results obtained for the chaotic attractor at $h = 4.5\ \mu$m (Figs. 9 and 10 [15]) are similar to those obtained for $h = 3.5\ \mu$m. The spatial distribution of the correlation dimension is again almost uniform, except for the surface effect which is much stronger in the present case and
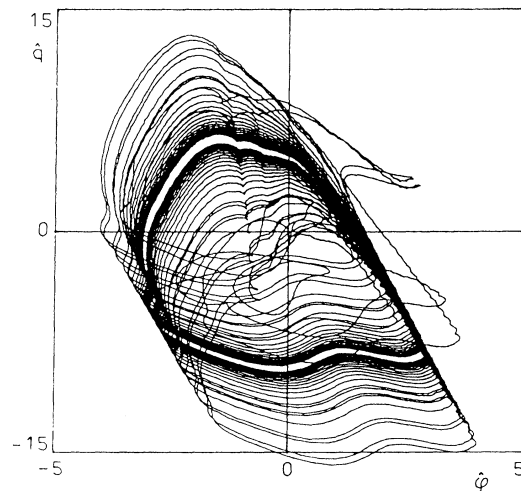

FIG. 13. Phase portrait of the midplane point in the wall for the chaotic attractor at $h = 5.0\ \mu$m.

FIG. 15. Phase portrait for the chaotic attractor at $h = 5.0\ \mu$m calculated at the surface of the film (grid point number 1).

much more symmetric (Fig. 11). The second scaling region is also obtained (Fig. 12)—this time at more grid points—but only at the surfaces the slopes of the two scaling regions are significantly different. The spatial uniformity of the attractor at $h=4.5$ μm obtained in the correlation-dimension calculations is again in good agreement with results obtained elsewhere by means of phase portrait analysis and power spectra [15].

The chaotic attractor (Figs. 13 and 14) obtained for $h=5.0$ μm was found elsewhere [15] to be spatially nonuniform: the phase portraits at or close to the surface of the material (Fig. 15) were different from those found close to the midplane of the film (Fig. 13). The correlation function curve for this attractor displays three scaling regions (Fig. 16). The slopes of these regions yield three values of correlation dimension at each grid point (Fig. 17: solid curve, larger length scales; pluses, intermediate length scales; crosses, smaller length scales). It can be seen that the differences between the values of the correlation dimension at different locations are now significantly larger. The regions around the parts of the wall which are 24 grid points away from the surfaces of the film had been previously found to be a boundary between two different chaotic regions in the wall [15]: the two at the surfaces of the film and the one around the midplane area. At these boundary regions a distinct phase portrait (Fig. 18) was obtained [15]. In Fig. 17 (solid curve) it can be seen that the correlation dimension has a maximum close to the boundary regions found in Ref. [15].

The correlation dimension from one of the scaling regions (smaller length scales, crosses in Fig. 17) is not a reliable measure of the statistics on the attractor since the scaling region, although sharply defined at many of the grid points, has a width of only three points on the $C(\epsilon)$ curve. At grid points 56 and 68 the secondary slope was not available. Yet the distribution of the value of this slope follows qualitatively the distribution given by the solid curve in Fig. 17. Thus, for the reconstructed space
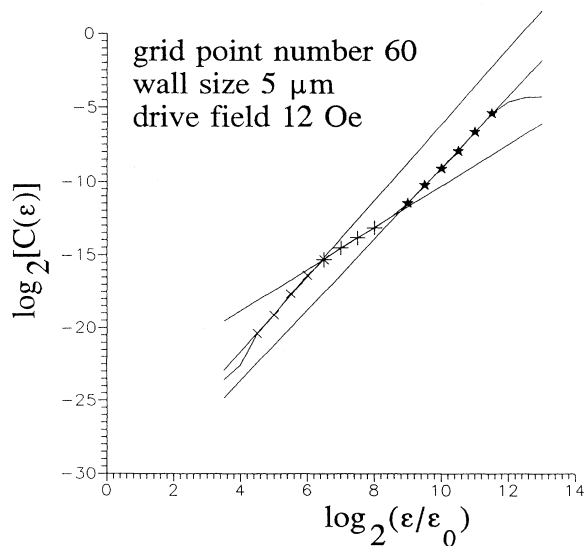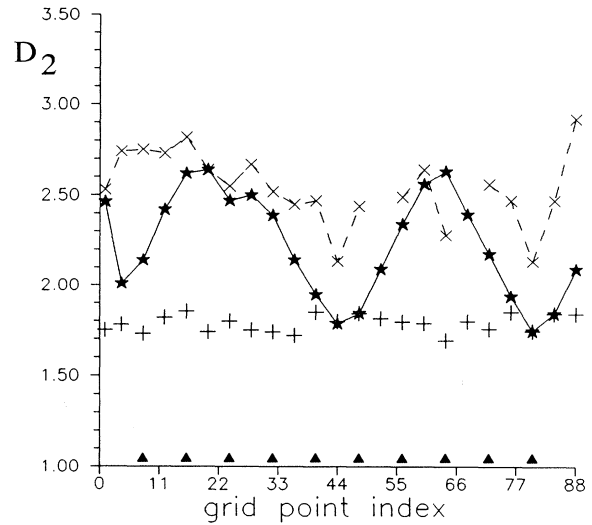

FIG. 17. Correlation dimensions D_2 for $h=5.0$ μm as function of position along the height of the wall. Symbols: ×, lower lengths scales; +, intermediate lengths scales; *, largest lengths scales; ▲, locations from which the physical space was constructed.

embedding, the spatial distribution of the correlation dimension seems to mirror the dynamics of the system: an increase in the dimension is obtained in those regions where two attractors border within the height of the wall and perturbed each other.

The third scaling region found for this case for the intermediate length scales of the $C(\epsilon)$ curve (pluses in Fig. 17) yielded a surprisingly uniform value of the slope. It is possible that the existence of this intermediate scaling region lying between the other two is a symptom of a bunching of the trajectory loops as they surround the repellor (the unstable fixed point representing the Walker motion of the wall [3]). As the radius ϵ is increased above a certain value, the hypersphere of the Grassberger-Procaccia algorithm encompasses a part of the attractor

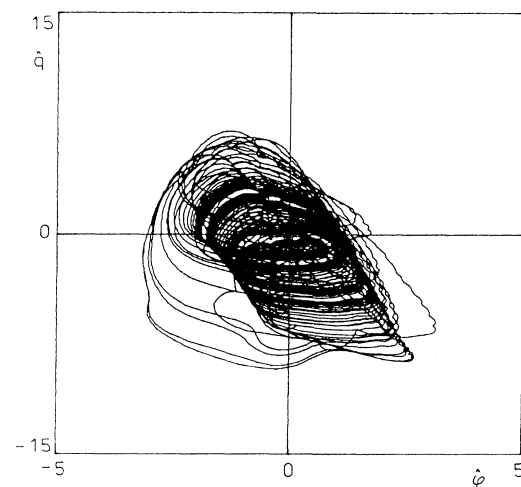FIG. 16. Correlation function $C(\epsilon)$ for $h=5.0$ μm calculated at grid point number 60.

FIG. 18. Phase portrait for the chaotic attractor at $h=5.0$ μm calculated at grid point number 24.

which is less frequently visited by the trajectory. For still larger ϵ, the hypersphere again enters a region where more trajectories are close together. This interpretation is borne out by the shape of the two-dimensional projections of the phase portraits (cf. Fig. 13, the midplane phase portrait) where two types of loops are visible: tighter ones around the point (0,0) (the repellor) and larger ones further away from it. It also explains the poorer quality of the slope $C(\epsilon)$ at smaller length scales (crosses in Fig. 17)—the solid curve in Fig. 17 was calculated on a better statics (larger number of points of the trajectory within the hypersphere).

B. Physical phase space

For the attractors at $h = 4.5$ and 5.0 μm the values of the correlation dimension obtained from physical space are an average of the spatial distribution of the correlation-dimension form reconstructed phase space. For the $h = 4.5$ μm a single scaling region is obtained with the correlation dimension of 2.44. For the $h = 5$ μm attractor three scaling regions were found with slopes 2.13, 1.4, and 2.05.

A rather surprising result is obtained for $h = 3.5$ μm, for which the physical-space calculation unexpectedly seems to fail for this spatially uniform attractor yielding also two scaling regions with slopes 1.97 and 2.35, which bracket the values of correlation dimension found for the reconstructed space calculation.

In general, the results found for the Bloch wall seem to agree with a remark by Babloyantz [20] based on a calculation of the correlation dimension from experimentally measured human electroencephalogram that the multichannel approach—an equivalent of the physical-space embedding used here—generally yields lower values than does the reconstructed phase space.

VI. CONCLUSIONS

The many-scale behavior found for two of the strange attractors analyzed should not be attributed to problems with statistical dependence of the points on the trajectory. The specific distortions of the $C(\epsilon)$ curves mentioned in the literature [17,23] and due to strong correlations between points on the trajectory were present in the calculation at an early stage when the original Grassberger-Procaccia algorithm with $K = 1$ and $P = N$ was used. The calculation presented here has been fine tuned by judicious use of the parameters—sampling time and delay time τ—so that the scaling regions obtained are best defined and their boundaries are sharp. Note also that, although rather elaborate corrections to the Grassberger-Procaccia algorithm (i.e., [23,24]) may make the distortion (the so-called "knee") of the $C(\epsilon)$ curves at higher embedding dimensions go away leaving a well-defined slope, often several scaling regions are obtained [cf. Figs. 5(b) and 6 in Ref. [24]).

In the calculations of correlations dimension presented above care was taken to treat data taken from all grid points of a given chaotic attractor equally. Thus, if a spatial distribution of the correlation dimension is obtained—especially when such a distribution is more pronounced at the surfaces of the material—this means

that the Takens theorem of phase-space reconstruction, when applied to a spatially extended system, yields a measure of the local properties of the system. This may come as a surprise since for maps and an ordinary differential equation the correlation dimension is expected to be just a single number—a measure of the complexity of the system as a whole. It may be surmised that if, for the reconstruction, a truly infinite length of the trajectory of the system were used (as indeed the Takens theorem assumes), then perhaps no spatial distribution would be obtained and a single number for the correlation dimension of the Bloch wall would result. Unfortunately, for real experimental situations as well as for computer experiments like the present calculation, the trajectory available is far from infinite. In the course of this study, the number of points used for the most spatially nonuniform case ($h = 5$ μm) was doubled from 5000 to 10 000. The spatial distribution did not change and only a scatter present in the values of the correlation dimension was diminished resulting in a smoother curve.

Due to the finite length of the time series used, the spatial distribution of correlation dimension discussed here is only a qualitative measure of the complexity of a spatially extended dynamical system. However, the above results are in agreement with the conclusions of the two-point correlation-density calculations [13,14] that, at least for a finite-length time series, the number of degrees of freedom is a local quantity. In any case, care should be taken during measurements in spatially extended systems as the placement of the measuring tool with respect to the symmetry of the system may be an important factor.

It is indeed not surprising that a different result should be obtained for the surface or boundary of a given system other than what is found for its interior. However, a stronger statement may be made. Stoop et al. [21] have found experimental indications that during avalanche breakdown in a semiconductor a gradual decoupling of different parts of the sample may occur leading to slightly different fractal dimensions. Similar behavior for the Bloch wall has been found in a numerical experiment earlier [15] (and partially reproduced here) in the case of the strange attractor at $h = 5$ μm. The phase portrait shown in Fig. 18 was attributed in Ref. [15] to an attractor which arises due to mutual perturbation of three attractors: the one obtained at the surface (Fig. 15), the one found in the midplane of the material (Fig. 13), and an adjacent (in parameter space) periodic attractor which some of the loops seen in Fig. 13 closely resemble. Consequently one should expect that the region of the wall where the attractor of Fig. 13 is found (about 24 grid points away from the surfaces) will have a larger number of degrees of freedom active and this is borne out by the results presented in Fig. 17. Other groups have also obtained two-scale behavior and have used this result to claim a spatially nonuniform character of the dynamics of the system studied (see, e.g., Figs. 2 and 3 of Sato, Sano, and Sawada [22] and accompanying discussion).

Since the strange attractors studied here for wall height $h = 3.5$, 4.5, and 5 μm give a single scale, a two-scale and a three-scale behavior, respectively, one natu-

rally wonders what will occur at still larger heights of the wall. The calculations for large wall sizes become cumbersome as more and more grid points must be used to retain accuracy while there is no good way to automate the finding of the scaling regions for each grid point studied. However, preliminary results for the strange attractor at $h = 6$ μm (106 grid points) show that only three scaling regions are found and the overall picture seems to be similar to that in Fig. 17. For this state many solitary waves are present at once in the wall structure [15], which seems to account for the fact that the calculated correlation dimensions at some points in the wall exceed 3.5. Calculation of the correlation dimension for still larger wall heights is planned.

For hydrodynamics, it has been shown that the correlation dimension of a spatially extended system may be seen as an extensive property of the system and as such will increase with system size [12–14,25]. It is interesting to note that in the case of the Bloch wall it is not so. Not only has the single-point correlation dimension not increased by more in amplitude than 15% with an increase of the size of the system by 2, but also the correlation dimension from physical space—a measure of the averaged or global dynamics of the system—has not increased

significantly. The reason is that with the increase of the size of the system studied here the number of coherent spatial structures (Bloch lines) has not increased in a dramatic way. Preliminary calculations indicate [26] that even for a much larger increase of the size of the system (up to at least 40 μm) the number of coherent spatial structures, although rising, does not increase dramatically and that a cascade of coherent structures with smaller and smaller length scales—to be expected in hydrodynamics—does not occur in the Bloch wall. Perhaps then, for systems with coherent spatial structures—the extensiveness of correlation dimension goes with the number of independent (as opposed to bound) coherent spatial structures present rather than with just the size of the system.

ACKNOWLEDGMENTS

[1] H. G. Schuster, *Deterministic Chaos—An Introduction* (Physik-Verlag, Weinheim, 1988).

[2] E. A. Overman, D. W. Maclaughin, and A. R. Bishop, Physica D **19**, 1 (1986).

[3] J. J. Żebrowski, Phys. Scr. **38**, 632 (1988).

[4] R. Kosiński and A. Sukiennicki, J. Magn. Magn. Mat. **104-107**, 331 (1992).

[5] A. Wolf, J. Swift, and L. Swinney, Physica D **16**, 285 (1985).

[6] P. Szephalusy, T. Tel. A. Csordas, and Z. Kovacs, Phys. Rev. A **36**, 3525 (1987).

[7] P. Grassberger and I. Procaccia, Phys. Rev. Lett. **50**, 5 (1983); **50**, 346 (1983).

[8] F. Takens, Phys. Rev. Lett. **51**, 14 (1980); **51**, 1265 (1980).

[9] A. Broomhead and G. King, in *Nonlinear Phenomena and Chaos* (Hilger, Bristol, 1986).

[10] P. Grassberger, Phys. Scr. **40**, 346 (1989).

[11] J. A. Vastano and H. L. Swinney, Phys. Rev. Lett. **60**, 1773 (1988).

[12] Y. Pomeau, C. R. Acad. Sci. Paris, Ser. II 7, 239 (1985).

[13] T. Kurz and G. Mayer-Kress, *The Physics of Phase Space. Nonlinear Dynamics and Chaos, Geometric Quantization, Wigner Function*, edited by Young Suh Kim and Woodford W. Zachary, Lecture Notes in Physics Vol. 278 (Springer, Berlin, 1987).

[14] G. Mayer-Kress and T. Kurz, Complex Syst. **1**, 821 (1987).

[15] J. J. Żebrowski and A. Sukiennicki, in *Deformations of Mathematical Structures: Surface Effects*, edited by J.

Ławrynowicz (Kluwer, Norwell, MA, in press).

[16] A. P. Malozemoff and J. C. Slonczewski, *Magnetic Domain Walls* (American New York, 1979).

[17] J. W. Havstad and C. L. Ehlers, Phys. Rev. A **39**, 2 (1989); **39**, 845 (1989).

[18] W. Lauterborn nd J. Holzfuss, Phys. Lett. **115**, 8 (1986); **115**, 369 (1986).

[19] J. J. Żebrowski, Phys. Rev. B **39**, 7205 (1989).

[20] A. Babloyantz, in *Chaos in Brain Function*, edited by E. Basar (Springer, Berlin, 1990).

[21] R. Stoop, J. Peinke, J. Parisi, Röhricht, and R. P. Huebener, Physica D **35**, 425 (1989).

[22] S. Sato, M. Sano, and Y. Sawada, Phys. Rev. A **37**, 5 (1988); **37**, 1679 (1988).

[23] J. Theiler, Phys. Rev. A **34**, 3 (1987); **34**, 2427 (1987).

[24] J. Kuo and J. C. Principe, in *Removing Artificial Correlation From Time Series for Dimension Estimation: Experimental Result*, Proceedings of the Conference on Measuring Chaos in the Human Brain, edited by D. Duke and W. Pritchard (World Scientific, Singapore, 1991).

[25] A. Brandstätter, H. L. Swinney, and G. T. Chapman, in *Dimensions and Entropies in Chaotic Systems—Quantification of Complex Behavior*, edited by G. Mayer-Kress, Springer Series in Synergetics Vol. 32 (Springer, Berlin, 1986).

[26] J. Żebrowski and A. Sukiennicki, in Proceedings of the Fifth Symposium on Statistical Physics Zakopane 1992 [Acta Phys. Pol. (to be published)].